

# JGR Space Physics

## RESEARCH ARTICLE

10.1029/2023JA031396

### Key Points:

- Jupiter's auroral bright spot emissions observed by Juno-Ultraviolet Spectrograph were simultaneously measured with the JADE, JEDI, Waves, and MAG instruments
- For each event, we observe characteristic changes in particle distributions, wave emissions, and magnetic field disturbances
- Whistler waves and electric currents appear to play a role in generating bright auroral polar spots

### Supporting Information:

Supporting Information may be found in the online version of this article.

### Correspondence to:

K. Haewsantati and S. Wannawichian,  
[K.Haewsantati@uliege.be](mailto:K.Haewsantati@uliege.be);  
[suwicha.w@cmu.ac.th](mailto:suwicha.w@cmu.ac.th)




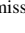






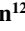




### Citation:

Haewsantati, K., Bonfond, B., Wannawichian, S., Gladstone, G. R., Hue, V., Greathouse, T. K., et al. (2023). Juno's multi-instruments observations during the flybys of auroral bright spots in Jupiter's polar aurorae. *Journal of Geophysical Research: Space Physics*, 128, e2023JA031396. <https://doi.org/10.1029/2023JA031396>

Received 14 FEB 2023

Accepted 14 JUL 2023

## Juno's Multi-Instruments Observations During the Flybys of Auroral Bright Spots in Jupiter's Polar Aurorae

K. Haewsantati<sup>1,2,3</sup> , B. Bonfond<sup>1</sup> , S. Wannawichian<sup>3,4</sup> , G. R. Gladstone<sup>5</sup>, V. Hue<sup>5,6</sup> , T. K. Greathouse<sup>5</sup>, D. Grodent<sup>1</sup> , Z. Yao<sup>1,7</sup> , J.-C. Gérard<sup>1</sup>, R. Guo<sup>1,8</sup> , S. Elliott<sup>9,10</sup> , B. H. Mauk<sup>11</sup> , G. Clark<sup>11</sup> , D. Gershman<sup>12</sup> , S. Kotsiaros<sup>13</sup> , W. S. Kurth<sup>9</sup> , J. Connerney<sup>12</sup> , J. R. Szalay<sup>14</sup> , and A. Phriksee<sup>3</sup>

<sup>1</sup>LPAP, STAR Institute, Université de Liège, Liège, Belgium, <sup>2</sup>Ph.D. Program in Physics, Department of Physics and Materials Science, Faculty of Science, Chiang Mai University, Chiang Mai, Thailand, <sup>3</sup>National Astronomical Research Institute of Thailand (Public Organization), Chiang Mai, Thailand, <sup>4</sup>Department of Physics and Materials Science, Faculty of Science, Chiang Mai University, Chiang Mai, Thailand, <sup>5</sup>Southwest Research Institute, San Antonio, TX, USA, <sup>6</sup>Aix-Marseille Université, CNRS, CNES, Institut Origines, LAM, Marseille, France, <sup>7</sup>Key Laboratory of Earth and Planetary Physics, Institute of Geology and Geophysics, Chinese Academy of Sciences, Beijing, China, <sup>8</sup>Laboratory of Optical Astronomy and Solar-Terrestrial Environment, Institute of Space Sciences, School of Space Science and Physics, Shandong University, Weihai, China, <sup>9</sup>Department of Physics and Astronomy, University of Iowa, Iowa City, IA, USA, <sup>10</sup>School of Physics and Astronomy, University of Minnesota, Minneapolis, MN, USA, <sup>11</sup>The Johns Hopkins University Applied Physics Laboratory, Laurel, MD, USA, <sup>12</sup>NASA Goddard Space Flight Center, Greenbelt, MD, USA, <sup>13</sup>DTU Space, Technical University of Denmark (DTU), Kongens Lyngby, Denmark, <sup>14</sup>Department of Astrophysical Sciences, Princeton University, Princeton, NJ, USA

**Abstract** Juno's arrival at Jupiter in 2016 revealed unprecedented details about Jupiter's ultraviolet aurorae thanks to its unique suite of remote sensing and in situ instruments. Here we present results from in situ observations during Juno flybys above specific bright auroral spots in Jupiter's polar aurora. We compare data observed by Juno-UVS, JEDI, JADE, Waves, and MAG instruments when Juno was magnetically connected to bright polar auroral spots (or their immediate vicinity) during perijove 3 (PJ3), PJ15, and PJ33. The highly energetic particles observed by JEDI show enhancements dominated by upward electrons, which suggests that the particle acceleration region takes place below the spacecraft. Moreover, brightness and upward particle flux were higher for the northern bright spot in PJ3 than the southern spots found in PJ15 and PJ33. In addition, we notice the intensification of whistler-mode waves at the time of the particle enhancements, suggesting that wave-particle interactions contribute to the acceleration of particles that cause the UV aurorae. The MAG data reveal magnetic perturbations during the PJ3 spot detection by Juno, which suggests the presence of significant field-aligned electric currents. While the stable positions of the bright spots in System III suggest that the phenomenon is fixed to the planet's rotation, the presence of field-aligned currents leaves the possibility of an origin rooted much farther in the magnetosphere.

## 1. Introduction

Jupiter's ultraviolet (UV) aurorae, the brightest of the solar system, are caused by high-energy particles precipitating along magnetic field lines and interacting with the neutral particles in Jupiter's upper atmosphere. The Jovian aurorae are usually divided into four components: the main emissions, the equatorward emissions, the polar emissions, and the satellite footprints. Each component exhibits different behaviors and morphologies depending on the specific processes from which they originate. In previous work, we studied a feature in the polar aurora, which we named a bright auroral spot (Haewsantati et al., 2021). This feature appears as a compact shape with a power on the order of 10 GW. We found that the bright spots usually take the form of a quasi-periodic pulsation fixed in System III longitude position during the sequence. The spots are mostly located near the edge of the swirl region (Grodent et al., 2003), within the polar emissions. We suggested the source possibly corotates with Jupiter according to their fixed positions. The bright spots are seen at all local times, which is inconsistent with the idea of the simple Earth-like cusp process (Pallier & Prangé, 2001), which would always be oriented toward noon. We note that the Earth's and Saturn's cusps can also be spread in local time under the right solar wind conditions (Arridge et al., 2016; Jasinski et al., 2014, 2016). However, Zhang et al. (2021) pointed out that the topology of Jupiter's magnetospheric cusp could be very complex. Therefore, we cannot exclude that the bright spot could be related to cusp-like processes in a complex and twisted polar magnetosphere.

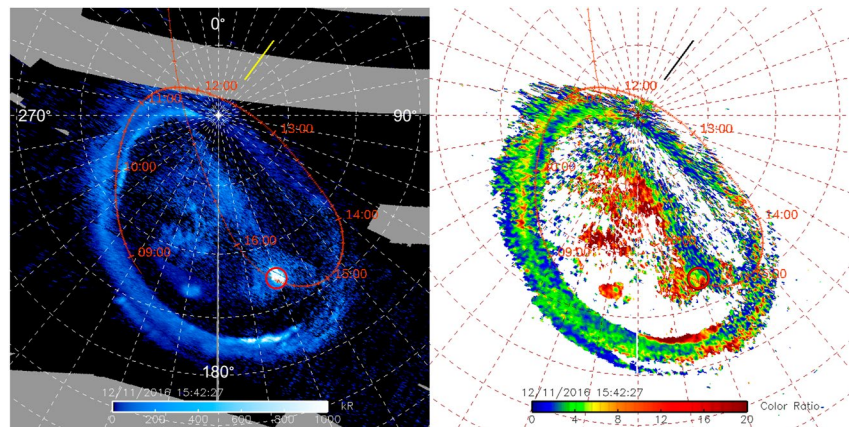
The Juno spacecraft carries a comprehensive suite of instruments dedicated to Jupiter's magnetosphere and aurorae (Bagenal et al., 2017). Juno moves along a very elliptical polar orbit and the close-up sequences, flying over Jupiter's pole from North to South, are typically named after their perijove (PJ) number. The morphology and spectral characteristics of the UV-aurorae are measured by the Ultraviolet Spectrograph (UVS) (Gladstone et al., 2017). UVS usually operates for several hours in each perijove, during which Juno is magnetically connected to various parts of the Jovian magnetosphere from the distant magnetotail when flying over the pole to the immediate neighborhood of Jupiter when flying over the equator and to various SIII longitudes as the planet rotates beneath it. The aurorae can also be observed remotely in the near-infrared by the Jupiter InfraRed Auroral Mapper (JIRAM) (Adriani et al., 2017). Juno in situ instruments provides critical insight into the magnetospheric processes leading to the Jovian aurorae. The plasma and energetic particles populations are measured with two instruments, the Jovian Auroral Distributions Experiment (JADE) (McComas et al., 2017) for the low-energy particles and the Jupiter Energetic-particle Detector Instrument (JEDI) (Mauk et al., 2017a) for the high-energy particles. The characteristics of electromagnetic waves and magnetic field are observed by the Waves and MAG instruments, respectively (Connerney et al., 2017; Kurth et al., 2017).

A series of multi-instrument studies of auroral processes have been carried out over the last few years. Several studies directly compared in situ particle measurements with UVS observations, for example, Gérard et al. (2019), Allegrini et al. (2020), Ebert et al. (2019), and Szalay et al. (2020). The comparisons have been made between precipitating electron flux measured by JEDI and the auroral intensity observed by UVS by Gérard et al. (2019). The results showed that the brightness of the main auroral emissions agrees well with the brightness computed from JEDI electron energy flux. The brightness inferred from the JEDI measurements is computed using a model-derived rule-of-thumb that 1 mW/m<sup>2</sup> electron energy flux produces about 10 kilo-Rayleighs (kR, 1 kR = 10<sup>9</sup> photon cm<sup>-2</sup>s<sup>-1</sup> into 4π steradians) of total unabsorbed FUV H<sub>2</sub> emission. However, in the polar region, not only is the observed upward particle energy flux larger than the downward flux (Mauk et al., 2017b), but also the downward flux is insufficient to produce the auroral UV emissions. Furthermore, the simultaneous observations of electron energy distributions from JADE and JEDI and the UV aurorae from UVS in the polar region during PJ5 (Ebert et al., 2019) showed that upward electron energy fluxes are greater than downward electron fluxes, the former being consistent with the UV emission recorded by UVS. Juno has found Jupiter's aurorae in the polar region to be much more complex than anticipated. From plasma measurement by JADE, Szalay et al. (2017) presented five distinct regions associated with Jupiter's polar regions. Subsequently, the polar particle environment has been characterized into multiple zones corresponding to the character of pitch angle distributions and the upward versus downward flux (Allegrini et al., 2020; Mauk et al., 2020). Additionally, JEDI detected intense upward electron beams at energies greater than 1 MeV and connected to the swirl region in the polar auroral region (Paranicas et al., 2018). Also, electron inverted-V and proton and ions inverted-V were found over the polar cap (Clark et al., 2017a, 2017b; Mauk et al., 2020; Mauk et al., 2017a, 2017b). Waves have observed intense upward whistler-mode waves above the polar region, correlating with detecting energetic electron precipitation by JEDI. The up-going electrons following an inverted-V pitch angle distribution are suggested to produce the upward whistler-mode waves (Elliott et al., 2020; Elliott et al., 2018a, 2018b; Kurth et al., 2018). Moreover, the interaction between these waves and particles could also play a role in the processes related to the auroral emissions.

We identified three unprecedented events during which Juno flew close to the field lines connecting to bright spot emissions. These events occurred during PJ3, PJ15, and PJ33, and we present the results from in situ observations of the bright spot emissions made by UVS, Waves, JEDI, JADE, and MAG instruments. A short summary of each instrument is presented in Section 2. The observational results related to each event are presented in Section 3 and are discussed in Section 4.

## 2. Instruments and Observations

UVS is a photon-counting imaging ultraviolet spectrograph. The instrument is operated in the spectral range between 68 and 210 nm, which covers the emissions in H<sub>2</sub> Lyman and Werner bands. A flat scan mirror at the instrument's entrance can look at a target within ±30° perpendicular to the spin plane. The “dog bone”-shaped slit consists of three contiguous segments with the field of views of 0.2° × 2.5°, 0.025° × 2°, and 0.2° × 2.5°. This study's spectral resolution is irrelevant because we only consider relatively broad bandwidth ranges to estimate the brightness, color ratios, and power emitted by H<sub>2</sub> in the UV domain. Hence, only the wide parts of



**Figure 1.** Polar projection showing a bright spot emission (red circle) in Jupiter's polar aurora as observed by Ultraviolet Spectrograph (left panel). The time presented here is the time of the last spin, where the bright auroral spot is detected. The grid consists of  $10^\circ$  spaced planetocentric parallels and SIII meridians. The right panel presents the color ratio, used as a proxy for the depth of the auroral emission.

the slit are used to maximize the signal-to-noise ratio. Each photon, detected during every 30-s spin of Juno, is attributed an  $X$  and  $Y$  position corresponding to the spectral dimension and spatial dimension, respectively (Gladstone et al., 2017; Greathouse et al., 2013; Hue et al., 2019). A spectral image of Jupiter's UV aurora is constructed based on the orientation of the scan mirror and the motion of the UVS field of view across the planet. A polar projection map is created assuming that the aurora are emitted at 400 km above the 1-bar pressure level (Bonfond et al., 2015). Since the scan mirror generally points to different locations on Jupiter for each spin near the closest approach or perijove, a global view of the aurora may be reconstructed from several consecutive spins in each closest approach or each perijove (PJ). In order to provide context for the in situ observations, we create a UV brightness map (left figure in Figure 1) to display a complete view of the auroral region by combining 100 spins, which cover approximately 50 min. On these maps, each spin is weighted differently so that the last spin covering a specific region dominates the others. This method provides the best compromise between coverage and dynamics (Bonfond et al., 2021). However, when we analyze the brightness and integrated power of a bright auroral spot, we only consider individual spin, as the bright spot is bright enough to get a good signal-to-noise ratio (Haewsantati et al., 2021). The power of the bright auroral spot is determined by the intensity of the last spin in which the spot brightens. In our analysis, we convert the photon count rate to brightness in kR, which, for the total unabsorbed  $H_2$  Lyman emissions and Werner bands, may be obtained by multiplying the total counts obtained in the 155–162 nm wavelength range with the conversion factor of 8.1, based on  $H_2$  synthetic spectrum (Gustin et al., 2013). The brightness is then multiplied by the surface area and the mean energy of a UV photon to obtain the power emitted. The analysis method of the bright spot surface area is described in the previous study by Haewsantati et al. (2021). Since the brightness is integrated over a relatively large auroral region, the shot noise uncertainty for a spot around 20 GW is a few percent and can thus be neglected (Gérard et al., 2019). The main uncertainty on the auroral brightness determination is due to the in-flight calibration of the instrument's effective area, which amounts to  $\sim 16\%$  (Hue et al., 2019). The FUV color ratio presented in this study is calculated by the ratio between the emission intensities of hydrogen molecules at wavelength range unaffected and affected by methane absorption,  $I(155\text{--}162\text{ nm})/I(125\text{--}130\text{ nm})$ .

Juno's Waves instrument measures the electric field spectra from 50 Hz to 41 MHz and the magnetic field spectra from 50 Hz to 20 kHz. The instrument consists of a dipole electric antenna, which is located perpendicular to the spacecraft's spin axis and  $x$ -axis, and a 15-cm long magnetic search coil sensor, whose axis is oriented parallel to the spacecraft's spin ( $z$ -axis) (Kurth et al., 2017). This study uses the Waves data with a sample rate of one spectrum per 1 s. However, the waves properties cannot be completely analyzed due to the limitations of single-axis measurement of the electric and magnetic field. Whether they are electromagnetic or quasi-electrostatic, the wave mode can be identified by the electro-to-magnetic field ratio ( $E/cB$ ), where  $c$  is the speed of light, along with characteristic frequencies of the plasma, such as the electron cyclotron frequency ( $F_{ce}$ ) and the electron plasma frequency ( $F_{pe}$ ), when detectable. The direction of the Poynting flux vector can be determined by comparing the phase between the electric and magnetic signals, measured by the Waves instruments, based on the assumption

that the Poynting flux direction of the waves can be either parallel or antiparallel to the background Jovian magnetic field (Kolmašová et al., 2018). For further analysis, the cyclotron frequencies can be calculated with in situ measurements from the Magnetic Field Investigation (MAG) instrument (Connerney et al., 2017).

The JEDI instrument is a particle detector, which measures the energy, angular, and compositional distributions of electrons ( $\sim 25$  to  $\sim 1,200$  keV) and ions ( $\sim 10$  keV to  $>1.5$  MeV for protons and  $\sim 150$  keV to  $>100$  MeV for oxygen and sulfur). The instrument consists of three sensors. Two sensors (JEDI-90 and JEDI-270) are mounted on the spacecraft deck with the field of view covering  $\sim 360^\circ$  along the plane roughly perpendicular to the Juno spin axis. JEDI-180 is oriented to cover nearly  $\sim 180^\circ$  along the Juno spin axis. Each sensor is comprised of a collimator, a time-of-flight (TOF) chamber, and a solid-state detector energy system (Mauk et al., 2017a). The pitch angles can be calculated using the magnetic vector provided by the magnetometer on board Juno (Connerney et al., 2017). Details for caveats related to JEDI data are discussed in Supporting Information of Mauk et al. (2018).

We can observe particles whose energies are lower than JEDI's energy range using the Jovian Auroral Distribution Experiment or JADE (McComas et al., 2017). The instrument consists of two subsystems, JADE-E for electron measurements and JADE-I for ion measurements. The JADE-E measures electrons with a 0.1–100 keV range. Two identical sensors are in use, each with  $120^\circ$  field of view, to instantaneously cover a total of  $240^\circ$  field of view in the azimuthal direction (perpendicular to the spin axis).

The Juno magnetometer (MAG) instrument consists of the Fluxgate Magnetometer and Advanced Stellar Compass (ASC) CCD imagers. The three components of the magnetic field vectors in the range of  $\sim 1$  nT to  $\sim 16 \times 10^5$  nT are measured by a pair of FGMs, together with the attitude determination system of the ASC. Depending on the distance between Juno and Jupiter, MAG can observe each magnetic field component with a sample rate of 64, 32, or 16 measurements per second. More details on the instruments are discussed in Connerney et al. (2017). Here we focus on the 1-s resolution magnetic field perturbations in each component during our focus time intervals. The magnetic perturbation is calculated by removing the estimated background field based on the Juno Reference Model through perijove 33 (JRM33) (Connerney et al., 2022) and the magnetodisc model (Connerney et al., 2020). The magnetic field perturbations in the perpendicular direction to the background magnetic field are then separated into the directions parallel and perpendicular to Juno's trajectory projected in the plane perpendicular to the magnetic field. We noted a significant shift between the observed magnetic field and the JRM33 (order18) + Con2020 model. Hence, we used a fifth-order polynomial fit to the data before and after the crossing to detrend the data to isolate the magnetic field deflection related to our event. For the interested readers, Figures S1–S3 in supporting information show the differences from the comparison between the magnetic field from observation, the JRM33 (order18) + Con2020 model, and the fifth-order polynomial fit during the crossing time.

### 3. Results

#### 3.1. PJ3 Event

Figure 1 shows 100-spin maps of the UVS brightness and color ratio of the bright spot emission found during PJ3 on 11 December 2016: the last spin, which contain the bright spot, was acquired at 15:42:27 UT. The red line represents the Juno footprint path according to the JRM33 model. According to the best-fit ellipse, the bright spot's center was located at latitude  $65.1^\circ$  N and  $158.9^\circ$  System III (SIII) longitude, with emitted power of  $\sim 71$  GW. This emission is found to be part of a bright spot emission sequence presented in Haewsantati et al. (2021). The UVS images show that Juno started to cross the bright spot emissions starting from  $\sim 15:38$  UT. However, brightness data are missing from 15:38 UT until 15:42 UT because of gaps in the UVS data stream and because the bright spot was in the area covered by the narrow slit. The in situ data were considered during the bright spot crossing, as shown in Figure 2. We highlighted four specific times, which are indicated by vertical dashed lines. Two black lines represent the times when Juno's magnetic footprint, indicated by the red curve on Figure 1, started to enter and exit the bright spot area, labeled by "I" for ingress and "E" for egress. The blue vertical dashed line, labeled "C," indicates when Juno's footprint is at its closest approach to the bright spot center. The pink vertical dashed line labeled "B" represents when the bright spot was the brightest, as seen by UVS, as shown in Figure 1.

Regarding the Waves observations, an intensification of whistler-mode hiss waves was observed from 15:36:30 UT until after 15:40:00 UT, as shown in the top panel in Figure 2 (zoom versions of the wave plots are available in supporting information Figure S4). This intensification started a few seconds before the enhancement of upward electrons (second panel). The  $E/cB$  ratio analysis (see Figure S5 in Supporting Information S1) shows that the

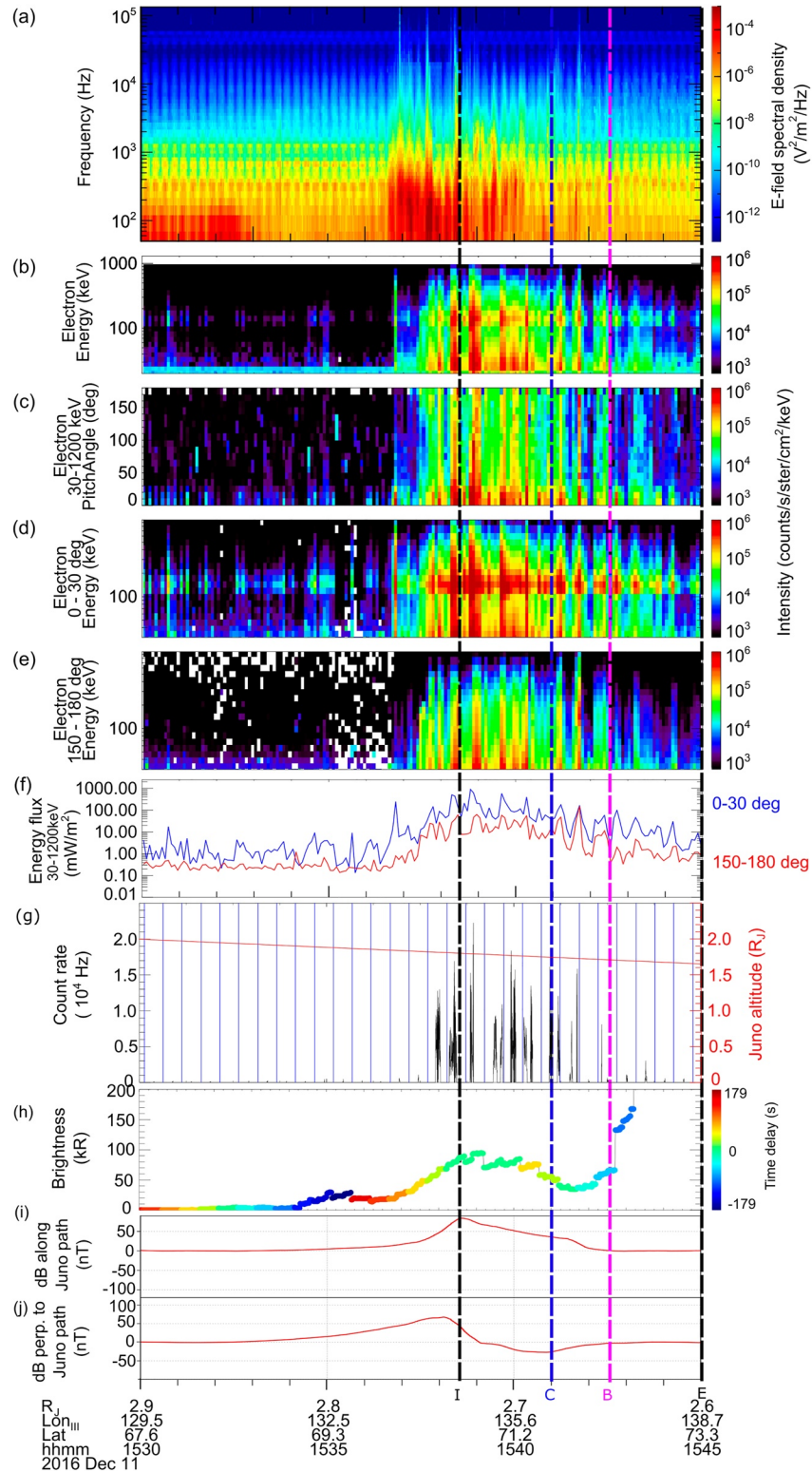


Figure 2.

waves are electromagnetic waves, indicated by the common value of electromagnetic whistler mode waves  $E/cB$  ratio between 1.0 and 2.0. Moreover, the Poynting flux analysis shows that, during the intensifications, a component of the Poynting flux direction is parallel to the magnetic field direction, implying that the waves propagate in the upward direction away from Jupiter for the northern hemisphere.

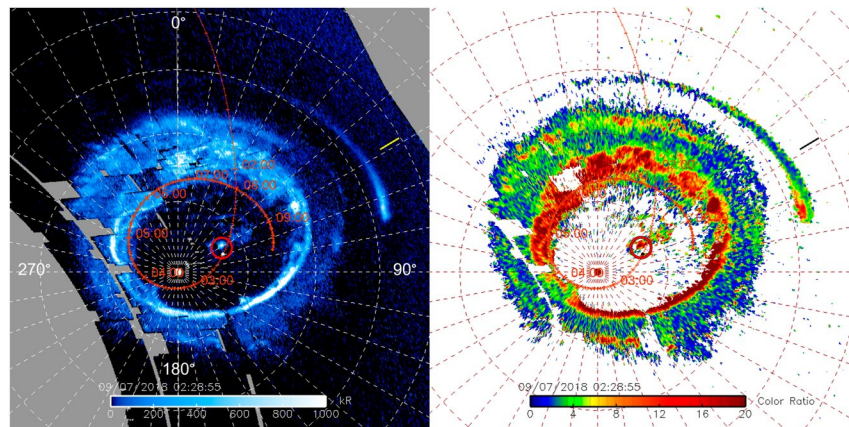
For JEDI data, we focus on the energy and pitch angle distributions of electrons as shown in panels (b)–(f) in Figure 2. The electron intensities started to increase at 15:37:47 UT, coinciding with the enhancement of the electric field spectral density (Figure 2a) until ~15:42 UT. The time interval between 15:37 UT to 15:42 UT covers when the Juno spacecraft's magnetic footprint passes closest to the bright spot position. The energy flux shows the quantitative measure (Figure 2f). Even though we used the most recent magnetic field model (JRM33), it should be noted that magnetic mapping uncertainty may prevent us from knowing the exact location of Juno's footprint relative to the bright spot. However, we believe that Juno flew close enough to see the connection between the particle flux intensification and the bright spot appearance. The particle distributions are dominated by upward electrons throughout the interval of interest. During the time that Juno flew across the bright spot position, that is, at around 15:38 - 15:40 UT, the upward electron flux reached ~900 mW/m<sup>2</sup> while the energy flux of downward electrons was <70 mW/m<sup>2</sup>. Panel (g) shows the Juno-UVS measurement of noise count rate, which is essentially related to >7 MeV electrons penetrating the instrument's shielding (Zhu et al., 2021). The blue vertical lines represent when the angle between UVS's boresight and the magnetic field points is minimal. This happens when UVS points away from Jupiter in the northern hemisphere and toward Jupiter in the southern hemisphere (c.f. PJ15 and PJ33). The red line presents Juno's altitude during this time interval. A 0 Hz rate generally indicates gaps in the recorded data stream. However, we note that the count rate peaks at levels much higher than the typical rate (20 kHz compared to ≤1 kHz), and these peaks appear simultaneous with the peaks of the JEDI energy flux (i.e., these values are never reached before 15:38 UT nor after 15:43 UT), indicating that the radiation noise detected by UVS corresponds the high energy tail of the electron distribution observed by JEDI. Panel (h) shows the brightness of Juno's footprint during the crossing and the time delay between the Juno time stamp and the actual UVS observation of the Juno footprint. The plot shows that, during the ingress (I) time, where the time delay is very short, meaning that the Juno's footprint brightness is observed simultaneously from UVS and JEDI, the brightness is approximately 90 kR. The average of 10–50 mW/m<sup>2</sup> of downward energy flux observed by JEDI (panel f) is sufficient to produce 100 kR of Juno's footprint brightness. The apparent brightness increases at the end of the interval took place much earlier (as indicated by the blue color). As it is not contemporaneous with the in situ measurements, it is irrelevant to the present discussion. No appreciable fluxes of lower energy plasma are observed by JADE, where only signatures of penetrating radiation are observed. As JEDI can measure the high energy charged particle environment, we focus on JEDI measurements for the remainder of this study.

Additionally, we studied the magnetic field perturbation at the time of the bright spot detection. The magnetic field perturbations (Figure 2 panels i and j) show magnetic deflections perpendicular to the field line. When decomposing to parallel and perpendicular components to Juno's trajectory projected on the perpendicular plane (as shown in Figures 2i and 2j, respectively) under the assumption that the currents are stationary, these deflections are the signature of downward currents. From Figure 2i, the maximum magnetic deflection is 75 nT, which results in approximately 1 MA of downward current if we assume that it flows along a field line mapping at the center of the bright spot. Even though the maximum amplitude of the magnetic deflection is about 0.2% relative to the ambient field, this data was observed at range 4 with a quantization step size of 3.12 nT, meaning that the perturbations are well resolved.

### 3.2. PJ15 Event

For the second identified event, a bright spot was found during PJ15, for the spin centered on 02:28:55 UT on 7 September 2018. In Figure 3, the bright spot's center position is 82.8° S and 58.1° SIII with emitted power of

**Figure 2.** Observations of electric field spectral density and 5-s bin of electron energy distributions observed during PJ3: (a) the electric field spectral density observed by the Waves instrument, (b) total electron energy distributions, (c) pitch angle distributions, (d) energy distributions for upward electrons (pitch angles 0°–30°), (e) energy distributions for downward electrons (pitch angles 150°–180°), and (f) energy fluxes for upward (0°–30°, blue line) and downward (150°–180°, red line) electrons in the 30–1,200 keV energy range. The horizontal band centered around 160 keV is a well-known instrumental effect documented in Mauk et al. (2018). Panel (g) shows the penetrating particle count rate measured by Juno-UVS. A zero count rate generally indicates a gap in the data stream. The vertical blue solid lines show the minima of the angle between the Ultraviolet Spectrograph (UVS) boresight and the magnetic field. The evolution of Juno's altitude is represented by the red line. Panel (h) shows the Juno's footprint brightness with the time delay. Panels (i) and (j) are magnetic field deviations observed by MAG in the directions along (parallel) and perpendicular to the Juno trajectory, respectively. The vertical dashed lines indicate the times when (I) Juno started to cross the bright spot (ingress), (C) Juno footprint was closest to the bright spot center, (B) UVS took the image of a bright spot as shown in Figure 1, and (E) the time of egress.

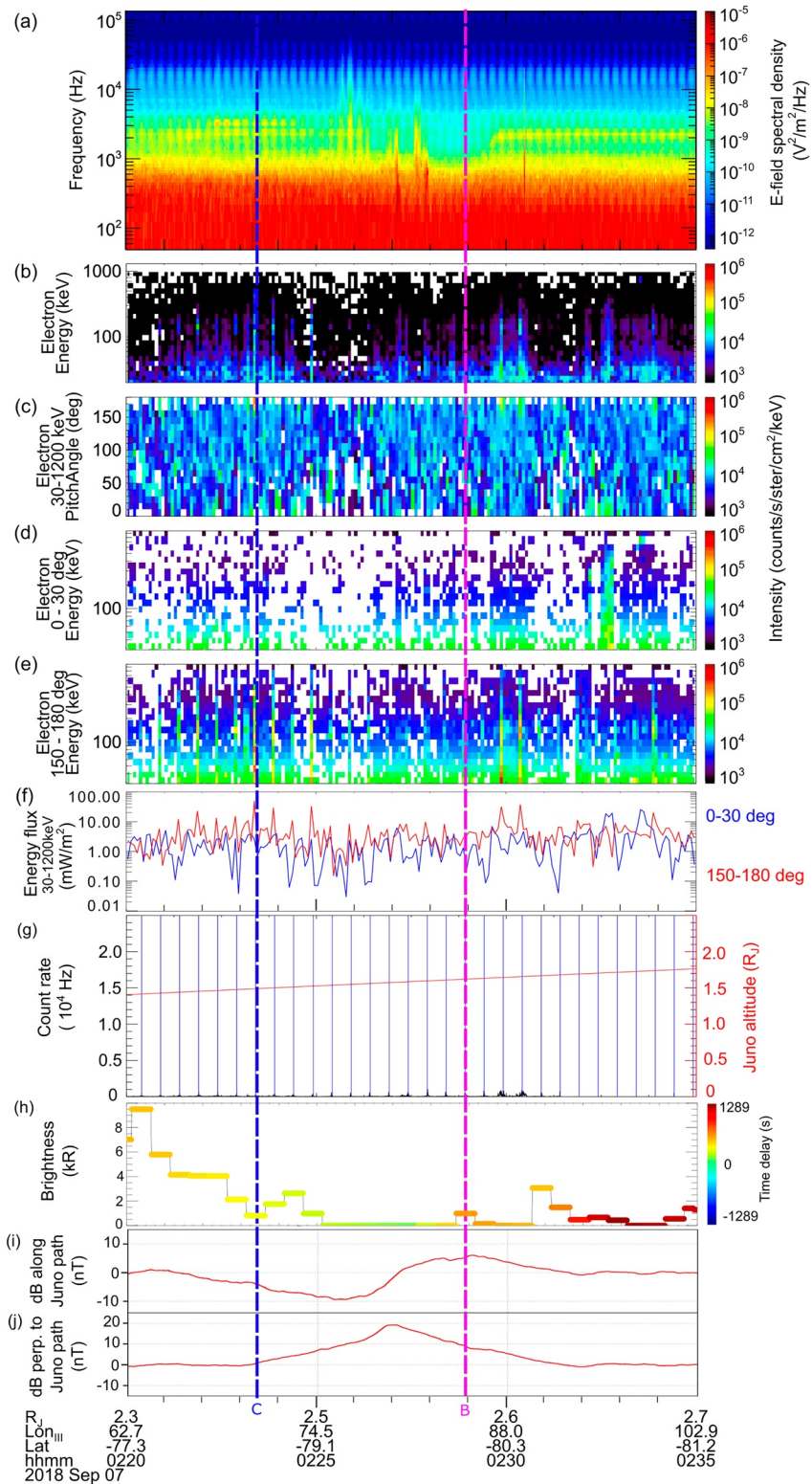


**Figure 3.** The polar projections with the same coordinates as Figure 1 show bright spot emission and the color ratio distribution in Jupiter's polar aurora as observed by Ultraviolet Spectrograph (UVS) from 100-spin where the last spin was when the bright spot was observed by the UVS.

~6 GW, previously presented in Haewsantati et al. (2021) and characterized by a high color ratio (around 15), indicating high-energy particles precipitating into the atmosphere. In this event, based on the JRM09 magnetic field model (Connerney et al., 2018), the bright spot position and the Juno position were very close. From the recent JRM33 model, while the bright spot was farther from Juno's footprint, the spacecraft still flew close to the bright spot emissions a few minutes before the UVS detection of the bright spot. Hence, we are still convinced that the faint signatures in the particle and Waves instruments recorded by Juno are related to the bright spot event. The electric field spectral density observed by the Waves instrument (Figure 4a and Figure S6 in supporting information) also shows the intensifications of Whistler-mode waves similar to those observed during PJ3. The  $E/cB$  ratio (see Figure S7) and the Poynting flux analysis imply that the detected waves are electromagnetic and anti-parallel to the magnetic field direction, indicating that waves were traveling upward away from Jupiter's southern hemisphere. The waves intensified before 02:28 UT, during the time that Juno flew close to bright spot emission indicated by a blue vertical dashed line (C). Next, the waves were damped during 02:28–02:30 UT when the bright spot was seen by UVS, indicated by a pink vertical dashed line (B).

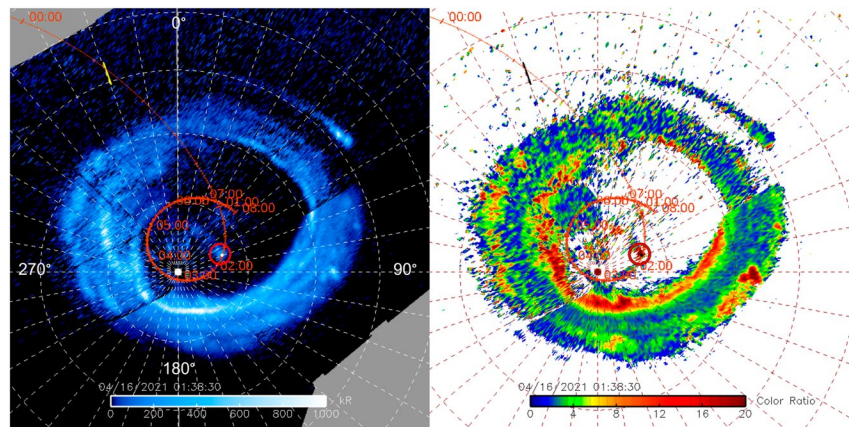
Regarding the pitch angle distribution, the JEDI energy flux in Figure 4 shows the same trend as in PJ3, in which the upward electrons dominated during the time interval of interest. However, the energy distribution shows only small fluctuations, with (1) an intensification dominated by upward electrons just before 02:25 UT, that is, right before Waves observed its intensification and near the time when Juno's footprint is closest to the bright spot emission, and (2) two intensifications near 02:30 UT at the time when UVS took an image of the bright spot at its brightest. Panels (e) and (f) clearly show that the enhancements were from upward electrons at ~02:23 UT and near 02:30 UT. The upward electron energy flux at the closest approach time indicated by the vertical dashed line (C) is ~50 mW/m<sup>2</sup>, while the downward electron energy flux is ~5 mW/m<sup>2</sup>. In addition, the upward electrons' energy flux of two peaks at 02:30 UT is 30–40 mW/m<sup>2</sup>, while the energy flux of downward electrons is <5 mW/m<sup>2</sup>. These energy fluxes of 30–40 mW/m<sup>2</sup> are lower than those observed during the PJ3 event, in agreement with the lower emitted power recorded by UVS. Panel (g) shows that the UVS count rate peaks at the blue vertical lines, representing the times when UVS's line of sight points toward Jupiter. The count rate is very low (possibly corresponding to a few Far-UV photons hitting the detector) and does not indicate any atypical radiation noise level. The Juno's footprint brightness plot (panel h) shows a long delay between the UV acquisition time and the other Juno observations. Therefore, we cannot determine whether the observed downward particles are sufficient to produce Juno's footprint brightness. A magnetic field deflection associated with this event was recorded in both components (Figures 4i and 4j), but their amplitudes are small (<20 nT).

It must be noted that this data was observed at range 4 with a quantization step size of 3.12 nT as in PJ3. In addition, this deflection is less than 0.1% relative to the ambient field. Therefore, the magnetic field deflection might be less obvious than that in PJ3. However, if we considered the same analysis of magnetic field perturbation direction as discussed in PJ3, these fluctuations imply the downward currents as well. In summary, the in situ signatures during the crossing are less prominent than those during the PJ3, partly because of the lower emitted



**Figure 4.** Observations of electric field spectral density and 5-s bin of electron energy distributions observed during PJ15, each panel is the same observation described in Figure 2. For the southern hemisphere, electrons with pitch angles 150°–180° and 0°–30° are upward and downward electrons, respectively. The energy fluxes (f) of upward electrons are presented by a red line and a blue line for downward electrons. Panels (g–j) and two vertical dashed lines, (C) and (B), are the same as in Figure 2.





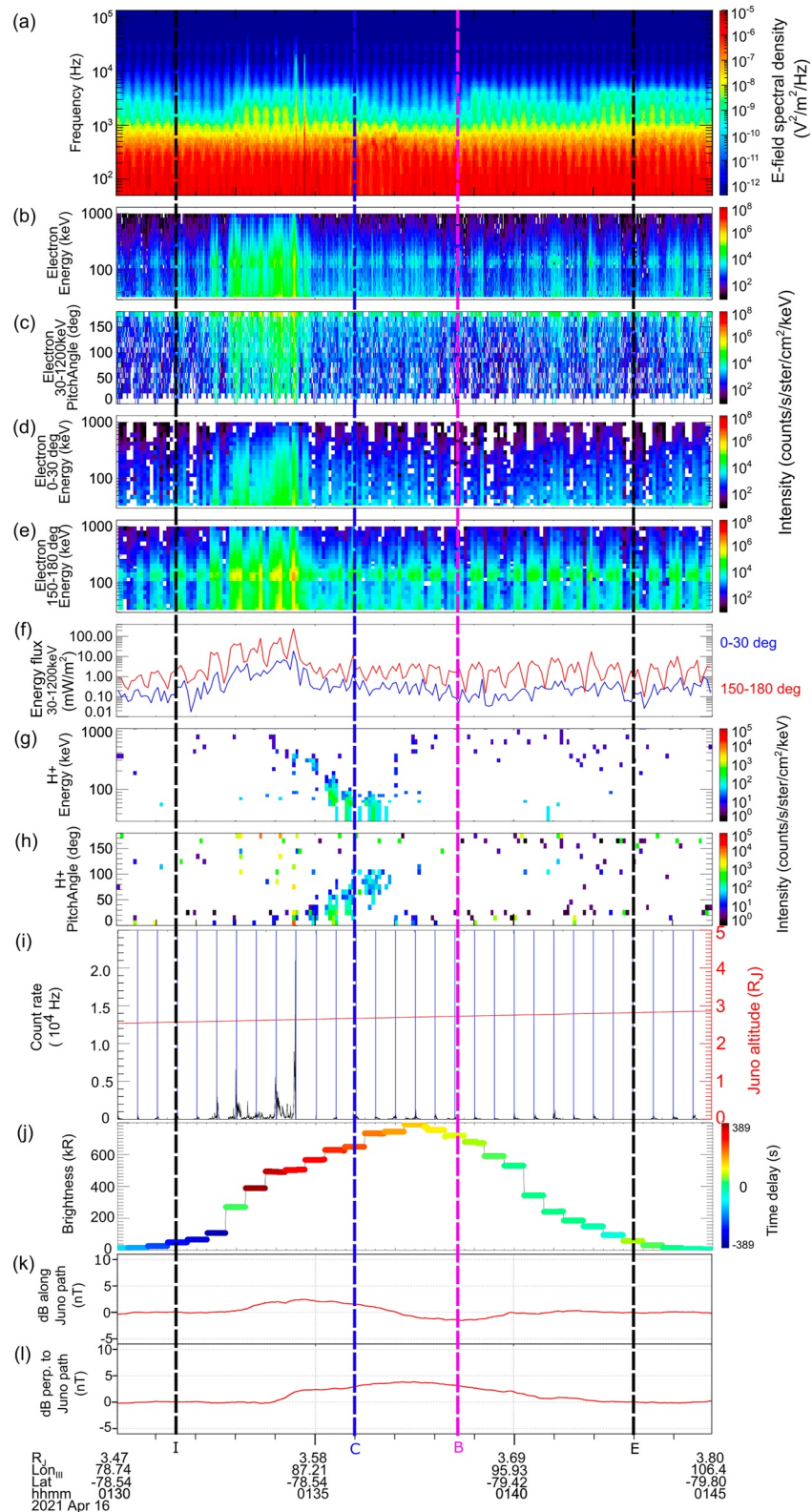
**Figure 5.** When the spacecraft flew close to the bright spot position during PJ33 on 16 April 2021, the polar projection shows bright spot emission in Jupiter's polar aurorae (left) and color ratio (right) as observed by Ultraviolet Spectrograph combined from 100-spin, with the last spin centered on 01:38:30 UT. The coordinates are the same as described in Figure 1.

power recorded by UVS (indicative of a weaker event), combined with the crossing distance further away from the bright spot center in PJ15.

### 3.3. PJ33 Event

The third event is a southern bright spot found during PJ33, as shown in Figure 5. The bright spot was seen at 01:38:30 UT on 16 April 2021 with a power of  $\sim 10$  GW at the center's position of  $83.5^\circ$  S and  $65.1^\circ$  SIII. The magnetic field deflection measured by the MAG instrument represents less than 0.01% of the ambient field at the time of the waves intensifications and electron enhancements during PJ33. It is thus not considered significant (Figures 6j and 6k). The electric field spectral density plot from Waves observations (Figure 6a, see details in supporting information Figure S8-S9) shows some intensifications above the proton cyclotron frequency, which is the Whistler-mode wave, at  $\sim 01:33$ – $01:37$  UT. However, there are no burst waveforms for the Poynting flux analysis. Therefore, the direction of the Poynting flux cannot be determined during this time interval.

An enhancement of the electron flux took place at  $\sim 01:33$  UT– $01:35$  UT, as shown in the JEDI plots (Figures 6b–6h). This event occurred during the time at which Juno crossed the bright spot emission (from the start of crossing to the closest approach to the bright spot center presented by vertical dash lines (I) and (C), respectively.) The enhancement is seen in the upward polar electron beam data, whose energy is higher than 500 keV. Upward electrons were previously observed over the polar auroral region, though their intensity usually was more modest (Mauk et al., 2020). Moreover, the UVS count rates shown in panel (i) reach peak values far beyond 1 kHz (up to 20 kHz) in the same time interval as the electron flux enhancements observed by JEDI. As for the PJ3 case, this enhanced UVS radiation rate indicates that the electron population has a high energy tail beyond 7 MeV. While the data stream during PJ3 was often interrupted, preventing firm conclusions about the orientation of the relativistic electrons, here, we can see that the peaks occur when the UVS points toward Jupiter (c.f. the blue lines), which indicates that the relativistic electrons go away from the planet. Furthermore, a zoom on this radiation noise shows a bursty behavior, similar to the bar code patterns described in Bonfond et al. (2018). JEDI measured an enhancement in the proton flux at  $\sim 01:35$  UT. Protons first moved downward, and then the low-energy protons with perpendicular pitch angles became more dominant. At the same time, the electron energy flux decreased after 01:35 UT and remained small during the UVS bright spot detection time (01:38 UT). During 01:39–01:42 UT when the shortest time delay of Juno's footprint brightness was detected, the downward electron flux ( $0.1$  mW/m<sup>2</sup>) at Juno position appears insufficient to produce 200–450 kR Juno footprint brightness. However, as shown in Table 1, the altitude of Juno during PJ33 was even higher than during PJ3 and PJ15. This suggests that the processes accelerating particles downward to the aurora and upward to the magnetosphere took place below the spacecraft. Finally, it is also noteworthy that the time of the most intense bright spot emissions does not exactly correspond to the time of the most intense upward particle flux. This indicates that Juno did not cross the field line connected to the bright spot when the UV-emitted power was maximum.



**Figure 6.** Observations of electric field spectral density by Waves and particle distributions made by JEDI instrument during PJ33. Panel (a–f) have similar descriptions as Figure 2, and particle directions are similar as described in 4. The proton energy and pitch angle distributions are shown in panels (g and h), respectively. The last four panels (i–l) and four vertical dashed lines are the same as in Figure 2.

**Table 1**  
*Summary Data for the Bright Spot In Situ Observation*

	PJ3	PJ15	PJ33
Date	11 Dec 2016	7 Septem 2018	16 April 2021
Juno footprint position (Lat, SIII Lon) <sup>a</sup>	(64.17°, 160.12°)	(-81.63°, 58.92°)	(-82.95°, 63.37°)
Juno altitude (R <sub>J</sub> ) <sup>a</sup>	1.70–1.65	1.40–1.45	2.58–2.60
Closest approach time (UT)	15:40:56	02:23:24	01:35:59
UVS observing time at brightest bright spot (UT)	15:42:27	02:28:55	01:38:30
Bright spot center position (Lat, SIII Lon)	(65.06°, 159.67°)	(-82.83°, 58.14°)	(-83.15°, 65.15°)
Bright spot power by UVS (GW) <sup>b</sup>	71.65	5.58	10.81
JEDI	Electron direction and enhancement time	Upward, two peaks (31.9 and 37.4 at time ~02:30 UT)	Upward during 01:33 UT–01:35 UT
	Maximum electron energy flux (mW/m <sup>2</sup> )	49.62 at 02:23:22 UT	860.52 at 01:34:29 UT
	Electron direction <sup>b</sup>	Upward	Upward
	Average electron energy flux (mW/m <sup>2</sup> ) <sup>c</sup>	3.33	2.63
	Proton direction	Upward	Upward then perpendicular
Waves	Whistler-mode intensification wave direction	02:26 UT–02:28 UT upgoing	01:33 UT–01:37 UT no analysis
MAG		A perturbation with small amplitude during 15:38 UT–15:42 UT	No significant deflection

<sup>a</sup>At closest approach. <sup>b</sup>At the UVS observing time. <sup>c</sup>Average ( $\pm 10$  s) during UVS observing time.

#### 4. Discussions and Conclusions

We present in situ and UV imaging observations during the brightening of bright spot emissions. The summary and comparison of the data from all instruments are shown in Table 1. The crossing time duration, the time in which Juno's path, according to JRM33, crosses the bright spot area, is 4–5 min for PJ3 and PJ15 and 12 min for PJ33. On the other hand, the brightness variation time interval of the emission bright spot, ~5 min (Haewsantati et al., 2021), is comparable to the crossing time. We have to consider this timing information when interpreting the data set. Based on the UVS data, the PJ3 emitted power is seven times more energetic than the PJ15 and PJ33 events. No discernible plasma signatures were observed below 50 keV in JADE, where only signatures of penetrating radiation were observed. Moreover, the enhancements of upward electron flux observed by JEDI are found in all three events. In all three cases, the bright spot, which is the signature of an intense flux of down-going particles, also corresponds to the enhanced electron fluxes in the upward direction. We note that the energy flux and the bright spot power for PJ3 are relatively high compared to the other two cases. The dominance of upward electrons combined with intense auroral emissions suggests that most of the electron acceleration occurs between the spacecraft and the planet, in both directions along the field lines.

The strong magnetic field deflection detected during PJ3 is most probably an indicator of significant (~1 MA) downward field-aligned currents on field lines connected to the bright spot. However, it should be noted that the magnetic perturbations in PJ15 and, more significantly, PJ33 do not show strong signatures as found in PJ3. Therefore, magnetospheric field-aligned currents do not appear as a necessary condition for bright spot emissions.

Regarding the wave-particle interactions, the upgoing whistler-mode waves have been related to the upward energetic electron beams in the Jovian polar cap (Elliott et al., 2020). Moreover, the upgoing electrons were suggested to be stochastically accelerated by the broadband whistler mode waves (Elliott et al., 2020; Elliott et al., 2018a). The concurrent intensifications observed in the JEDI and Waves data in PJ3, PJ15, and PJ33 support these arguments. We notice that whistler-mode waves occurred a few seconds before detecting an upward electron enhancement during PJ3. This enhancement started when Juno flew close to the bright spot position. In addition, the intensification of whistler-mode waves happened nearly simultaneously with electron enhancement in the PJ33 event. For PJ15, we also found that, where the altitude increases with time, the Whistler-mode waves were first enhanced and then damped for ~2 min. The time of wave enhancement corresponds to the time when Juno's footprint is closest to the bright spot center. Afterward, the bright spot was detected by the UVS, which took place at the time of wave damping. This behavior suggests that energy transfer between waves and particles occurs, as discussed in Elliott et al. (2018b). According to this theory, waves are generated close to the planet (i.e., at smaller radial distances) and then propagate along the magnetic field lines toward higher altitudes to become damped, transferring their energy to the electrons, which can then be accelerated. Since the bright spots were detected during the same time of the wave damping and followed by electron enhancements, the bright spot possibly appeared during the wave-particle enhancement. We suggest that these waves contribute to the acceleration of particles that cause UV emissions.

In addition, we see the burst of penetrating of electrons from the Juno-UVS measurements of count rates during the Juno bright spot flyby (Figures 2g, 4g, and 6i), which shows that the counts rates peak at the same time as the wave-particle enhancements for all three events. These concurrent results show a relative increase in the flux of upgoing particles seen in UVS and JEDI. One hypothesis is that we see the high energy tail of the particles related to the upward electron and upgoing whistler mode waves interaction as described by Elliott et al. (2018b).

It must be noted that there are possible time delays between UVS observation and wave and particle observations, which could explain the time differences between wave and particle enhancements and bright spot detection. Several scenarios are proposed, as follows. First, if we suppose that Juno was crossing magnetic field lines mapping to the bright spot, the observation times of the waves and particles should be prior to the bright spot emission time since waves and particles should take some time to travel from the spacecraft to the bright spot position beneath the spacecraft. To estimate how long the particles would travel, the travel times of a 100 keV electron and a 100 keV proton for a distance ~1.5  $R_J$  from the spacecraft to the bright spot position are 0.6 and 25 s, respectively. In contrast, the wave travel time is even shorter. As a result, the travel times of waves and particles should not cause the time differences between UVS spots and wave-particle enhancement detections. As a comparison, the spin period of the spacecraft is 30 s, which is longer than the travel time of even the protons. Second, the bright spot evolves with time, and the UVS image might capture it with a different

brightness or extent compared to the time of the field line crossing. This source of uncertainty would explain the mismatch in intensity rather than a time difference. Finally, the mapping from the magnetic model (JRM33 (order 18) + Con2020) might need to be more accurate. This error could be translated into a time delay.

Overall, for the processes related to the bright spot emissions, intense field-aligned currents do not seem to be a necessary condition for bright spot emissions, as only a weak signature was observed on PJ15, during which Juno only skimmed the field lines connected to the bright spot. No significant current was found during PJ33, for which the crossing took place closer to the center of the phenomenon. Interestingly, the currents identified for PJ3 and PJ15 were in the downward direction, consistent with an up-going electron flux larger than the down-going one, as measured by JEDI. We note that it is not the first time that larger up-going electron fluxes (compared to down-going fluxes) are found on field lines connected to auroral emissions in Jupiter's polar region (Ebert et al., 2017; Gérard et al., 2019; Mauk et al., 2017b). Furthermore, the fact that the bright spots are almost fixed in System III (Haewsantati et al., 2021) indicates that the processes giving rise to them are anchored to the planet. With supporting information from Waves (presence of Whistler mode waves) and JEDI (up-ward electron beam), wave-particle interactions associated with Whistler mode waves (Elliott et al., 2018b) appear as the most plausible process causing the particle acceleration leading to the auroral bright spot emission. However, two recent alternative scenarios should also be taken into consideration: (a) magnetic reconnection at Jupiter's near-planet polar magnetosphere, which could generate high-energy electron beams (Masters et al., 2021), and (b) the broadband acceleration due to the presence of an ionospheric Alfvén resonator or IAR (Lysak et al., 2021). In order to better identify the root cause for these intriguing bright spot emissions, further information could be found by looking deeper into the high-resolution magnetohydrodynamic simulations of the Jovian magnetosphere and the tangling of the magnetic flux tubes above the poles (see, e.g., Zhang et al., 2021). Other promising investigations would result from the future flybys over the bright spot through or below the particle acceleration region, sampling the downgoing particles and providing a direct link between the particle's behaviors and the auroral emissions.

#### Acknowledgments

The authors are grateful to NASA and contributing institutions, which have made the Juno mission possible. We thank Masafumi Imai for providing the Juno footprint tracing. We also thank a community code project: Magnetospheres of the Outer Planets Group Community Code (Vogt et al., 2022; Wilson et al., 2022) for providing the code to compute Jupiter's magnetic field and the magnetodisc model (<https://github.com/rjwilson-LASP/PSH> and <https://github.com/marissav06/con2020>). K. Haewsantati would like to acknowledge for Science Achievement Scholarship of Thailand and the Ph.D. program in Physics at Chiang Mai University. K. Haewsantati and S. Wannawichian are financially supported by the National Astronomical Research Institute of Thailand (NARIT). Additional support was from Thailand Science Research and Innovation grant RTA6280002. B. Bonfond is a Research Associate of the Fonds de la Recherche Scientifique - FNRS. B. Bonfond, D. Grodent, and J.-C. Gérard are funded by the Belgian Federal Science Policy Office (BELSPO) via the PRODEX Program of the European Space Agency (ESA). Z. Yao was supported by the National Science Foundation of China (Grant 42074211) and the Key Research Program of the Institute of Geology and Geophysics CAS (Grant IGGCAS-201904). J. R. Szalay was supported by Juno's NASA contract NNM06AA75C. The research at the University of Iowa is supported by NASA through Contract 699041X with Southwest Research Institute.

#### Data Availability Statement

All data used herein can be found in the Planetary Data System (PDS) (<https://pds.nasa.gov>). Ultraviolet Spectrograph (UVS) data can be obtained from [https://pds-atmospheres.nmsu.edu/cgi-bin/getdir.pl?dir=DATA&volume=jnouv3\\_3001](https://pds-atmospheres.nmsu.edu/cgi-bin/getdir.pl?dir=DATA&volume=jnouv3_3001) (Trantham, 2014). Waves survey data can be found in <https://pds.nasa.gov/ds-view/pds/viewDataset.jsp?dsid=JNO-E/J/SS-WAV-3-CDR-SRVFULL-V2.0> (Kurth & Piker, 2022). Juno Magnetometer data can be found in <https://pds-ppi.igpp.ucla.edu/search/view/?f=yes&id=pds://PPI/JNO-J-3-FGM-CAL-V1.0> (Connerney, 2022). JEDI data can be obtained from <https://pds-ppi.igpp.ucla.edu/search/view/?f=yes&id=pds://PPI/JNO-J-JED-3-CDR-V1.0> (Mauk, 2022). Jovian Auroral Distributions Experiment data may be found in [https://pds-ppi.igpp.ucla.edu/search/view/?f=yes&id=pds://PPI/JNO-J\\_SW-JAD-3-CALIBRATED-V1.0](https://pds-ppi.igpp.ucla.edu/search/view/?f=yes&id=pds://PPI/JNO-J_SW-JAD-3-CALIBRATED-V1.0) (Allegrini et al., 2022).

#### References

- Adriani, A., Filacchione, G., Di Iorio, T., Turrini, D., Noschese, R., Cicchetti, A., et al. (2017). JIRAM, the Jovian Infrared Auroral Mapper. *Space Science Reviews*, 213(1), 393–446. <https://doi.org/10.1007/s11214-014-0094-y>
- Allegrini, F., Mauk, B., Clark, G., Gladstone, G. R., Hue, V., Kurth, W. S., et al. (2020). Energy flux and characteristic energy of electrons over Jupiter's main auroral emission. *Journal of Geophysical Research: Space Physics*, 125(4), e2019JA027693. <https://doi.org/10.1029/2019JA027693>
- Allegrini, F., Wilson, R., Ebert, R., & Loeffler, C. (2022). Juno J/SW Jovian auroral distribution calibrated V1.0 [Dataset]. NASA Planetary Data System: Planetary Plasma Interactions Node. <https://doi.org/10.17189/1519715>
- Arridge, C. S., Jasinski, J. M., Achilleos, N., Bogdanova, Y. V., Bunce, E. J., Cowley, S. W. H., et al. (2016). Cassini observations of Saturn's southern polar cusp. *Journal of Geophysical Research: Space Physics*, 121(4), 3006–3030. <https://doi.org/10.1002/2015JA021957>
- Bagenal, F., Adriani, A., Allegrini, F., Bolton, S. J., Bonfond, B., Bunce, E. J., et al. (2017). Magnetospheric science objectives of the Juno mission. *Space Science Reviews*, 213(1–4), 219–287. <https://doi.org/10.1007/s11214-014-0036-8>
- Bonfond, B., Gladstone, G. R., Grodent, D., Gérard, J.-C., Greathouse, T. K., Hue, V., et al. (2018). Bar code events in the Juno-UVS data: Signature ~10 MeV electron microbursts at Jupiter. *Geophysical Research Letters*, 45(22), 12108–12115. <https://doi.org/10.1029/2018GL080490>
- Bonfond, B., Gustin, J., Gérard, J.-C., Grodent, D., Radioti, A., Palmaerts, B., et al. (2015). The far-ultraviolet main auroral emission at Jupiter – Part 2: Vertical emission profile. *Annales Geophysicae*, 33(10), 1211–1219. <https://doi.org/10.5194/angeo-33-1211-2015>
- Bonfond, B., Yao, Z. H., Gladstone, G. R., Grodent, D., Gérard, J.-C., Matar, J., et al. (2021). Are dawn storms Jupiter's auroral substorms? *AGU Advances*, 2(1), e2020AV000275. <https://doi.org/10.1029/2020AV000275>
- Clark, G., Mauk, B. H., Haggerty, D., Paranicas, C., Kollmann, P., Rymer, A., et al. (2017a). Energetic particle signatures of magnetic field-aligned potentials over Jupiter's polar regions. *Geophysical Research Letters*, 44(17), 8703–8711. <https://doi.org/10.1002/2017GL074366>
- Clark, G., Mauk, B. H., Paranicas, C., Haggerty, D., Kollmann, P., Rymer, A., et al. (2017b). Observation and interpretation of energetic ion conics in Jupiter's polar magnetosphere. *Geophysical Research Letters*, 44(10), 4419–4425. <https://doi.org/10.1002/2016GL072325>

- Connerney, J. E. P. (2022). Juno MAG Calibrated Data J V1.0 [Dataset]. NASA Planetary Data System: Planetary Plasma Interactions Node. <https://doi.org/10.17189/1519711>
- Connerney, J. E. P., Benn, M., Bjarno, J. B., Denver, T., Espley, J., Jorgensen, J. L., et al. (2017). The Juno magnetic field investigation. *Space Science Reviews*, 213(1), 39–138. <https://doi.org/10.1007/s11214-017-0334-z>
- Connerney, J. E. P., Kotsiaros, S., Oliverson, R. J., Espley, J. R., Joergensen, J. L., Joergensen, P. S., et al. (2018). A new model of Jupiter's magnetic field from Juno's first nine orbits. *Geophysical Research Letters*, 45(6), 2590–2596. <https://doi.org/10.1002/2018GL077312>
- Connerney, J. E. P., Timmins, S., Hecceg, M., & Joergensen, J. L. (2020). A Jovian magnetodisc model for the Juno Era. *Journal of Geophysical Research: Space Physics*, 125(10), e2020JA028138. <https://doi.org/10.1029/2020JA028138>
- Connerney, J. E. P., Timmins, S., Oliverson, R. J., Espley, J. R., Joergensen, J. L., Kotsiaros, S., et al. (2022). A new model of Jupiter's magnetic field at the completion of Juno's Prime Mission. *Journal of Geophysical Research: Planets*, 127(2), e2021JE007055. <https://doi.org/10.1029/2021JE007055>
- Ebert, R. W., Allegrini, F., Bagenal, F., Bolton, S. J., Connerney, J. E. P., Clark, G., et al. (2017). Spatial distribution and properties of 0.1–100 keV electrons in Jupiter's polar auroral region. *Geophysical Research Letters*, 44(18), 9199–9207. <https://doi.org/10.1002/2017GL075106>
- Ebert, R. W., Greathouse, T. K., Clark, G., Allegrini, F., Bagenal, F., Bolton, S. J., et al. (2019). Comparing electron energetics and UV brightness in Jupiter's northern polar region during Juno Perijove 5. *Geophysical Research Letters*, 46(1), 19–27. <https://doi.org/10.1029/2018GL081129>
- Elliott, S. S., Gurnett, D. A., Kurth, W. S., Clark, G., Mauk, B. H., Bolton, S. J., et al. (2018a). Pitch angle scattering of upgoing electron beams in Jupiter's polar regions by whistler mode waves. *Geophysical Research Letters*, 45(3), 1246–1252. <https://doi.org/10.1002/2017GL076878>
- Elliott, S. S., Gurnett, D. A., Kurth, W. S., Mauk, B. H., Ebert, R. W., Clark, G., et al. (2018b). The acceleration of electrons to high energies over the Jovian polar cap via whistler mode wave-particle interactions. *Journal of Geophysical Research: Space Physics*, 123(9), 7523–7533. <https://doi.org/10.1029/2018JA025797>
- Elliott, S. S., Gurnett, D. A., Yoon, P. H., Kurth, W. S., Mauk, B. H., Ebert, R. W., et al. (2020). The generation of upward-propagating whistler mode waves by electron beams in the Jovian polar regions. *Journal of Geophysical Research: Space Physics*, 125(6), e2020JA027868. <https://doi.org/10.1029/2020JA027868>
- Gérard, J.-C., Bonfond, B., Mauk, B. H., Gladstone, G. R., Yao, Z. H., Greathouse, T. K., et al. (2019). Contemporaneous observations of Jovian energetic auroral electrons and ultraviolet emissions by the Juno spacecraft. *Journal of Geophysical Research: Space Physics*, 124(11), 8298–8317. <https://doi.org/10.1029/2019JA026862>
- Gladstone, G. R., Persyn, S. C., Eterno, J. S., Walther, B. C., Slater, D. C., Davis, M. W., et al. (2017). The ultraviolet Spectrograph on NASA's Juno mission. *Space Science Reviews*, 213(1–4), 447–473. <https://doi.org/10.1007/s11214-014-0040-z>
- Greathouse, T. K., Gladstone, G. R., Davis, M. W., Slater, D. C., Versteeg, M. H., Persson, K. B., et al. (2013). Performance results from in-flight commissioning of the Juno ultraviolet Spectrograph (Juno-UVS). In *UV, X-ray, and gamma-ray Space instrumentation for astronomy XVIII* (Vol. 8859, p. 88590T). International Society for Optics and Photonics. <https://doi.org/10.1117/12.2024537>
- Grodent, D., Clarke, J. T., Waite, J. H., Cowley, S. W. H., Gérard, J.-C., & Kim, J. (2003). Jupiter's polar auroral emissions. *Journal of Geophysical Research*, 108(A10), 1366. <https://doi.org/10.1029/2003JA010017>
- Gustín, J., Gérard, J. C., Grodent, D., Gladstone, G. R., Clarke, J. T., Pryor, W. R., et al. (2013). Effects of methane on giant planet's UV emissions and implications for the auroral characteristics. *Journal of Molecular Spectroscopy*, 291, 108–117. <https://doi.org/10.1016/j.jms.2013.03.010>
- Haewsantati, K., Bonfond, B., Wannawichian, S., Gladstone, G. R., Hue, V., Versteeg, M. H., et al. (2021). Morphology of Jupiter's polar auroral bright spot emissions via Juno-UVS observations. *Journal of Geophysical Research: Space Physics*, 126(2), e2020JA028586. <https://doi.org/10.1029/2020JA028586>
- Hue, V., Gladstone, G. R., Greathouse, T. K., Kammer, J. A., Davis, M. W., Bonfond, B., et al. (2019). In-flight characterization and calibration of the Juno-ultraviolet Spectrograph (Juno-UVS). *The Astronomical Journal*, 157(2), 90. <https://doi.org/10.3847/1538-3881/aaf36>
- Jasinski, J. M., Arridge, C. S., Coates, A. J., Jones, G. H., Sergis, N., Thomsen, M. F., et al. (2016). Cassini plasma observations of Saturn's magnetospheric cusp. *Journal of Geophysical Research: Space Physics*, 121(12), 12047–12067. <https://doi.org/10.1002/2016JA023310>
- Jasinski, J. M., Arridge, C. S., Lamy, L., Leisner, J. S., Thomsen, M. F., Mitchell, D. G., et al. (2014). Cusp observation at Saturn's high-latitude magnetosphere by the Cassini spacecraft. *Geophysical Research Letters*, 41(5), 1382–1388. <https://doi.org/10.1002/2014GL059319>
- Kolmašová, I., Imai, M., Santolik, O., Kurth, W. S., Hospodarsky, G. B., Gurnett, D. A., et al. (2018). Discovery of rapid whistlers close to Jupiter implying lightning rates similar to those on Earth. *Nature Astronomy*, 2(7), 544–548. <https://doi.org/10.1038/s41550-018-0442-z>
- Kurth, W. S., Hospodarsky, G. B., Kirchner, D. L., Mokrzycki, B. T., Averkamp, T. F., Robison, W. T., et al. (2017). The Juno waves investigation. *Space Science Reviews*, 213(1), 347–392. <https://doi.org/10.1007/s11214-017-0396-y>
- Kurth, W. S., Mauk, B. H., Elliott, S. S., Gurnett, D. A., Hospodarsky, G. B., Santolik, O., et al. (2018). Whistler mode waves associated with broadband auroral electron precipitation at Jupiter. *Geophysical Research Letters*, 45(18), 9372–9379. <https://doi.org/10.1029/2018GL078566>
- Kurth, W. S., & Piker, C. W. (2022). Juno E/J/S/SS Waves Calibrated Survey Full Resolution V2.0 [dataset]. NASA Planetary Data System: Planetary Plasma Interactions Node. <https://doi.org/10.17189/1520498>
- Lysak, R. L., Song, Y., Elliott, S., Kurth, W., Sulaiman, A. H., & Gershman, D. (2021). The jovian ionospheric alfvén resonator and auroral particle acceleration. *Journal of Geophysical Research: Space Physics*, 126(12), e2021JA029886. <https://doi.org/10.1029/2021JA029886>
- Masters, A., Dunn, W. R., Stallard, T. S., Manners, H., & Stawarz, J. (2021). Magnetic reconnection near the planet as a possible driver of Jupiter's mysterious polar auroras. *Journal of Geophysical Research: Space Physics*, 126(8), e2021JA029544. <https://doi.org/10.1029/2021JA029544>
- Mauk, B. H. (2022). JEDI calibrated (CDR) data JNO J JED 3 CDR V1.0 [Dataset]. NASA Planetary Data System: Planetary Plasma Interactions Node. <https://doi.org/10.17189/1519713>
- Mauk, B. H., Clark, G., Gladstone, G. R., Kotsiaros, S., Adriani, A., Allegrini, F., et al. (2020). Energetic particles and acceleration regions over Jupiter's polar cap and main aurora: A broad overview. *Journal of Geophysical Research: Space Physics*, 125(3), e2019JA027699. <https://doi.org/10.1029/2019JA027699>
- Mauk, B. H., Haggerty, D. K., Jaskulek, S. E., Schlemm, C. E., Brown, L. E., Cooper, S. A., et al. (2017a). The Jupiter Energetic Particle Detector Instrument (JEDI) investigation for the Juno mission. *Space Science Reviews*, 213(1), 289–346. <https://doi.org/10.1007/s11214-013-0025-3>
- Mauk, B. H., Haggerty, D. K., Paranicas, C., Clark, G., Kollmann, P., Rymer, A. M., et al. (2017b). Juno observations of energetic charged particles over Jupiter's polar regions: Analysis of monodirectional and bidirectional electron beams. *Geophysical Research Letters*, 44(10), 4410–4418. <https://doi.org/10.1002/2016GL072286>
- Mauk, B. H., Haggerty, D. K., Paranicas, C., Clark, G., Kollmann, P., Rymer, A. M., et al. (2018). Diverse electron and ion acceleration characteristics observed over Jupiter's main aurora. *Geophysical Research Letters*, 45(3), 1277–1285. <https://doi.org/10.1002/2017GL076901>
- McComas, D. J., Alexander, N., Allegrini, F., Bagenal, F., Beebe, C., Clark, G., et al. (2017). The Jovian Auroral Distributions Experiment (JADE) on the Juno mission to Jupiter. *Space Science Reviews*, 213(1), 547–643. <https://doi.org/10.1007/s11214-013-9990-9>
- Pallier, L., & Prangé, R. (2001). More about the structure of the high latitude Jovian aurorae. *Planetary and Space Science*, 49(10), 1159–1173. [https://doi.org/10.1016/S0032-0633\(01\)00023-X](https://doi.org/10.1016/S0032-0633(01)00023-X)

- Paranicas, C., Mauk, B. H., Haggerty, D. K., Clark, G., Kollmann, P., Rymer, A. M., et al. (2018). Intervals of intense energetic electron beams over Jupiter's poles. *Journal of Geophysical Research: Space Physics*, *123*(3), 1989–1999. <https://doi.org/10.1002/2017JA025106>
- Szalay, J. R., Allegrini, F., Bagenal, F., Bolton, S., Clark, G., Connerney, J. E. P., et al. (2017). Plasma measurements in the Jovian polar region with Juno/JADE. *Geophysical Research Letters*, *44*(14), 7122–7130. <https://doi.org/10.1002/2017GL072837>
- Szalay, J. R., Allegrini, F., Bagenal, F., Bolton, S. J., Bonfond, B., Clark, G., et al. (2020). Alfvénic acceleration sustains Ganymede's footprint tail aurora. *Geophysical Research Letters*, *47*(3), e2019GL086527. <https://doi.org/10.1029/2019GL086527>
- Trantham, B. (2014). JUNO Jupiter UVS calibrated data archive V1.0 [Dataset]. NASA Planetary Data System: Atmospheres Node. <https://doi.org/10.17189/C32J-7R56>
- Vogt, M., Wilson, R., Provan, G., Kamran, A., James, M., Brennan, M., & Cowley, S. (2022). Con2020 - Current sheet model code. Retrieved from <https://github.com/marissav06/con2020>
- Wilson, R., Vogt, M., Provan, G., Kamran, A., James, M., Brennan, M., & Cowley, S. (2022). PSH: Planetary spherical harmonics community code. Retrieved from <https://github.com/rjwilson-LASP/PSH>
- Zhang, B., Delamere, P. A., Yao, Z., Bonfond, B., Lin, D., Sorathia, K. A., et al. (2021). How Jupiter's unusual magnetospheric topology structures its aurora. *Science Advances*, *7*(15), eabd1204. <https://doi.org/10.1126/sciadv.abd1204>
- Zhu, B., Lindstrom, C., Jun, I., Garrett, H., Kollmann, P., Paranicas, C., et al. (2021). Jupiter high-energy/high-latitude electron environment from Juno's JEDI and UVS science instrument background noise. *Nuclear Instruments and Methods in Physics Research Section A: Accelerators, Spectrometers, Detectors and Associated Equipment*, *1002*, 165244. <https://doi.org/10.1016/j.nima.2021.165244>